Title
Efficient numerical methods for multiscale crowd dynamics with emotional contagion

Journal
Mathematical Models and Methods in Applied Sciences, 27(01)

ISSN
0218-2025

Authors
Wang, Li
Short, Martin B
Bertozzi, Andrea L

Publication Date
2017

DOI
10.1142/s0218202517400073

Peer reviewed

Efficient numerical schemes for multiscale crowd dynamics with emotional contagion

Li Wang* Martin Short † Andrea L. Bertozzi ‡

September 1, 2015

Abstract

In this paper, we develop two efficient numerical methods for a multiscale kinetic equation in the context of crowd dynamics with emotional contagion [2]. In the continuum limit, the mesoscopic kinetic equation produces a natural Eulerian limit with nonlocal interactions. However, such limit ceases to be valid when the underlying microscopic particle characteristics cross, corresponding to the blow up of the solution in the Eulerian system. One method is to couple these two situations – using Eulerian dynamics for regions without characteristic crossing and kinetic evolution for regions with characteristic crossing. For such a hybrid setting, we provide a regime indicator based on the macroscopic density and fear level, and propose an interface condition via continuity to connect these two regimes. The other method is based on a level set formulation for the continuum system. The so-derived level set equation shares similar forms as the kinetic equation, and it successfully captures the multi-valued solution in velocity, which implies that the multi-valued solution other than the viscosity solution should be the physically relevant ones for the continuum system. Numerical examples are presented to show the performance of these new methods.

1 Introduction

Multiscale phenomena find applications in a broad range of scientific problems such as gasses out of thermodynamic equilibrium, turbulence in fluids, and radiative transfer with variational collision rate. In most of these situations, the majority of the domain can be characterized by the macroscopic model, except in some small regions where microscopic effect are important such as near the boundaries or shock layers. Moreover, the macroscopic model gives the most efficient description, as it resides in physical space and requires the lowest computational cost; compare this to the mesoscopic kinetic model that resides in phase space, and the microscopic model that records the evolution of each individual. Therefore, it is desirable to use the macroscopic model whenever possible, and to restrict the use of the kinetic model to only those locations where it is necessary.

To this aim, domain decomposition technology has been widely explored, especially in the context of neutron transport with a macroscopic diffusion limit [20, 19, 1, 38], the Boltzmann equation with

*Department of Mathematics, University of California, Los Angeles, 520 Portola Plaza, Los Angeles, CA 90095 (liwang@math.ucla.edu).

†Department of Mathematics, Georgia Institute of Technology, 686 Cherry Street, Atlanta, GA 30332-0160 (mbshort@math.gatech.edu)

‡Department of Mathematics, University of California, Los Angeles, 520 Portola Plaza, Los Angeles, CA 90095 (bertozzi@math.ucla.edu)

a Eulerian or Navier-Stokes limit [5, 28, 27], and the hyperbolic relaxation system with multiple relaxation times [25, 11]. At the same time, a hybrid scheme has gained popularity in multiscale kinetic equations as well for its automatic detection of different regimes; consult [15, 12, 13] and also [18] for a recent extension to better regime indicator and higher order coupling.

In this paper, we consider the contagion dynamics of panicking, moving crowds modeled in [2], whose kinetic description in one dimension takes the form

$$f_t + (qf)_x = \gamma \left((q - q^*)f\right)_q, \tag{1.1}$$

where $f(t, x, q)$ is the probability density depending on time t, position x, and local fear level q. The quantity $q^*(t, x)$ is the "average" fear level for location x at time t, and is computed as the mean fear level of individuals weighted by their distance from x:

$$q^*(t, x) = \frac{\int\int \kappa(|x - y|) f(t, y, q) q dq dy}{\int\int \kappa(|x - y|) f(t, y, q) dq dy}.$$

Here $\kappa(r)$ is the interaction kernel that decays with r and integrates to one. The continuum limit of (1.1) reads

$$\rho_t + (\rho\tilde{q})_x = 0, \qquad (\rho\tilde{q})_t + \left(\rho\tilde{q}^2\right)_x = \gamma\rho(q^* - \tilde{q}) \tag{1.2}$$

under the mono-kinetic distribution assumption (which will be specified later). Here $\rho(t, x)$ and $\tilde{q}(t, x)$ are the macroscopic density and bulk fear defined as

$$\rho(t, x) = \int f(t, x, q) dq, \qquad \rho\tilde{q}(t, x) = \int f(t, x, q) q dq. \tag{1.3}$$

The continuum equation (1.2) can be considered as a pressureless Euler equation augmented with a nonlocal alignment that acts as a regularization. There exists a critical threshold above which the system admits a global smooth solution [2, 37], which leads to a flocking in the long time limit for initial data with compact support [37]. Such critical threshold phenomenon is typical for nonlocal PDE, see for example [33] for a scalar conservation law. It is also shown in [2] that if the initial data is below a threshold, the solution has finite time blow up, which in analogy with the agent based model means the particle characteristics can cross. In this case, the continuum model fails and the kinetic model is necessary.

We develop here a hybrid method where a kinetic solver is switched on wherever the macroscopic description ceases to be valid. The microscopic and macroscopic variables are linked through the local equilibrium. However, unlike the Boltzmann equation with its hydrodynamic limit whose local equilibrium is a well-defined Maxwellian, the equilibrium here is a delta function in the velocity space, which makes any regime indicator that depends on it very sensitive to the way the delta function is approximated. To this end, we propose a *uniform* indicator that works for both transitions from kinetic to continuum and continuum to kinetic. It depends on the distance of $\tilde{q}$ and q^* that follows an asymptotic property of (1.1). A threshold on the magnitude of ρ is also placed to avoid mislabeling near the center of the shock.

On the other hand, since the failure of the continuum system lies in the blow up of density that comes from the formation of a shock in fear, it is desirable to design a scheme which is able to capture the *multi-valued* fear instead of the viscosity solution. This is also suggested by the particles system, as crossing of particle characteristics implies a multi-valued fear level. The study of numerical methods for computing multi-valued solutions is pervasive in different contexts, such as [26, 23, 16, 9, 10] and references therein. The methods basically fall into two categories: one is a

particle method and the other is a level set method. The particle method is easy to implement and free of numerical dissipation, but designing a robust recovery method of the point values from its particle approximation is a challenging task, and the computational cost is sometimes very high (in our case it is $O(N^2)$ with N being the number of particles). Here we take the level set formulation, and derive a level set equation for computing the multi-valued fear level. To compute the density, we derive another evolution equation based on a new function, which follows the same spirit as in [24]. This level set equation is of similar form as the kinetic equation, but a local level set method can be utilized to significantly reduce the computational cost in phase space.

The rest of the paper is organized as follows. In the next section we give a brief review of the contagion dynamics and provide a simple derivation to link the different levels of model hierarchy. Section 3 is devoted to the hybrid algorithms and contains the regime indicator, interface condition, and discretization. In Section 4, we develop a level set formulation for the continuum system, and in Section 5, we present several numerical examples to show the performance of these two schemes. Finally, the paper is concluded in Section 6.

2 Contagion dynamics with continuum limit

In this section, we briefly review the contagion dynamics in one dimension wherein the particle velocity is proportional to its fear level (we use fear and velocity interchangeably from now on), and provide a formal relationship between different levels of models. More precisely, the agent based model reads

$$\frac{dx_i}{dt} = q_i, \qquad \frac{dq_i}{dt} = \gamma(q_i^* - q_i), \qquad q_i^* = \frac{\sum_{j=1}^N \kappa_{i,j} q_j}{\sum_{j=1}^N \kappa_{i,j}}, \tag{2.1}$$

where $x_i(t)$ and $q_i(t)$ are the position and fear level for each particle, and $\kappa_{i,j} = \kappa(|x_i - x_j|)$ is parametrized by an interaction distance R that characterizes the space dependent interaction. Parameter γ describes the interaction strength and it may vary with particle for more general cases.

Now we present a formal derivation of the kinetic formulation via a mean field limit [7] and pass to a continuum description under a mono kinetic velocity distribution assumption. Denote the empirical distribution density

$$f^N = \frac{1}{N}\sum_{i=1}^N \delta(x - x_i(t))\delta(q - q_i(t)), \tag{2.2}$$

then under the condition that the particles remain in a fixed compact domain $(x_i(t), q_i(t)) \in \Omega \subset \mathbb{R}^2$ for all i and up to the time we consider, there exists a subsequence $\{f^{N_k}\}_k$ such that f^{N_k} converges to f in the $weak^*$-limit in space and velocity and point-wisely in time as $k \to \infty$. Now consider a test function $\psi \in C_0^1(\mathbb{R}^{2d})$, we have

$$\begin{aligned} \frac{d}{dt}\left\langle f^N, \psi \right\rangle &= \frac{d}{dt}\left\langle \frac{1}{N}\sum_{i=1}^N \delta(x - x_i(t))\delta(q - q_i(t)), \psi \right\rangle = \frac{1}{N}\sum_{i=1}^N \psi_x q_i + \psi_q \gamma(q_i^* - q_i) \\ &= \left\langle \psi_x q, f^N \right\rangle + \frac{\gamma}{N}\sum_{i=1}^N \psi_q \left(\frac{\sum_{j=1}^N \kappa_{i,j} q_j}{\sum_{j=1}^N \kappa_{i,j}} - q_i \right). \end{aligned} \tag{2.3}$$

Further,

$$\frac{1}{N}\sum_{j=1}^{N}\kappa(|x_i-x_j|)=\left\langle \kappa(|x_i-x_j|),\frac{1}{N}\delta(y-x_j)\right\rangle=\kappa*\rho_{f^N}(x_i),$$
$$\frac{1}{N}\sum_{j=1}^{N}\kappa(|x_i-x_j|)q_j=\left\langle \kappa(|x_i-x_j|),\frac{q}{N}\sum_{j=1}^{N}\delta(y-x_j)\delta(q-q_j)\right\rangle=\kappa*m_{f^N}(x_i),$$

where we have used the definitions

$$\rho_{f^N}(x)=\frac{1}{N}\sum_{i=1}^{N}\delta(x-x_i),\qquad m_{f^N}(x)=\left\langle q,\frac{1}{N}\sum_{j=1}^{N}\delta(x-x_j)\delta(q-q_j)\right\rangle=\frac{1}{N}\sum_{j=1}^{N}\delta(x-x_j)q_j.$$

Therefore (2.3) reads

$$\frac{d}{dt}\left\langle f^N,\psi\right\rangle=\left\langle \psi_x q,f^N\right\rangle+\gamma\left\langle f^N,\frac{\kappa*m_{f^N}}{\kappa*\rho_{f^N}}\psi_q-q\psi_q\right\rangle,$$

which leads to

$$f^N_t+(qf^N)_x=\gamma\left((q-q^*)f^N\right)_q,\qquad q^*=\frac{\int\int\kappa(|x-y|)f(y,q)qdqdy}{\int\int\kappa(|x-y|)f(y,q)dqdy}\tag{2.4}$$

via integration by parts. Then letting $N\to\infty$, we formally have the limiting kinetic equation

$$f_t+(qf)_x=\gamma\left((q-q^*)f\right)_q.\tag{2.5}$$

To further reduce the dimension, we take the moments of (2.5), which enables us to write the evolution of the macroscopic quantities: the mass density $\rho(t,x)$ and bulk fear level $\tilde{q}(t,x)$ defined in (1.3), and pressure $P(t,x)$ given by

$$P(t,x)=\int(q-\tilde{q})^2f(t,x,q)dq.\tag{2.6}$$

The resulting continuum equation reads

$$\rho_t+(\rho\tilde{q})_x=0,\qquad(\rho\tilde{q})_t+\left(\rho\tilde{q}^2+P\right)_x=\gamma\rho(q^*-\tilde{q}).\tag{2.7}$$

Now we assume that the particle distribution is mono-kinetic in velocity space, i.e.,

$$f(t,x,q)=\rho(t,x)\delta(q-\tilde{q}(t,x)),\tag{2.8}$$

then the pressure vanishes and (2.7) is rewritten as

$$\rho_t+(\rho\tilde{q})_x=0,\qquad(\rho\tilde{q})_t+(\rho\tilde{q}^2)_x=\gamma\rho(q^*-\tilde{q}),\qquad q^*=\frac{\int\kappa(|x-y|)\rho(y)\tilde{q}(y)dy}{\int\kappa(|x-y|)\rho(y)dy},\tag{2.9}$$

which can be considered as a pressure-less Euler equation with a nonlocal alignment. Note that, at least formally, in the limit of zero interaction radius and infinite interaction rate, that is, $\gamma\to\infty$ and $R\to 0$, system (2.9) reduces to the classical pressureless Euler equation modeling sticky particles in gas dynamics [6, 3], whose solution admits a $\delta-$singularity that has been well-understood analytically [22, 8, 3, 31, 32, 36] and numerically [4]. Here in (2.9), the nonlocal alignment can be

considered as a regularization to the $\delta-$singularity and may lead to a uniformly bounded solution for any time T under some appropriate assumption [33]. Consequently, the momentum equation in (2.9) is equivalent to the following non-conservative form

$$\tilde{q}_t + \tilde{q}\tilde{q}_x = \gamma(q^* - \tilde{q}). \tag{2.10}$$

For smoothed Riemann initial data, the readers are refereed to [2] for two formal theorems regarding the critical threshold behavior of the solutions. The more detailed analysis of system (2.9) is still lacking.

To end this section, we would like to mention the interesting results in [34] for self-organized dynamics, whose model in one dimension is the same as ours. In that paper, the authors focus on the long-time behavior (or so-called flocking behavior) that characterizes a long time "equilibrium" when all particles form into one cluster with the same speed. On the contrary, in this paper we are interested in capturing the transient behavior, especially when the particle characteristics can cross, whose long time behavior is not flocking. Moreover, we would like to treat different kinds of initial data, not just those with compact support as is considered in [34] (in analogy with the agent based model, compact support means a finite number of agents).

3 Hybrid scheme via kinetic formation

The high dimensionality makes the kinetic equation expensive to compute, while the continuum system fails to capture the multi-value solution in the presence of the crossing of characteristics. It is therefore desirable to construct a hybrid scheme that automatically becomes a kinetic solver whenever the particles tend to cross and stays as a macroscopic solver when particles are kept a certain distance away.

3.1 Regime indicators

Our first task is to provide a formal justification of the mono-kinetic distribution that links the kinetic equation (2.5) with continuum system (2.9). Consider a space homogeneous toy model

$$f_t = \frac{1}{\epsilon}\left[(q - q^*)f\right]_q, \qquad \int_{\mathbb{R}} f(0,q)dq = 1, \tag{3.1}$$

where q^* is any *constant*. The following proposition highlights the relaxation of the kinetic solution f towards the mono-kinetic distribution (2.8) at the fast ϵ time scale.

Proposition 1. *Let $f(t,q) > 0$ be the solution to the initial value problem of the space homogeneous equation (3.1). Assume $f(t,q)$ decays faster than $\frac{1}{|q|^2}$ as $|q| \to \infty$. Then f converges to $\delta(q - \tilde{q}(t))$ and $\delta(q - q^*)$ formally as $t \to \infty$, where $\tilde{q} = \int f(t,q)qdq$. Therefore, $\tilde{q}(t) \to q^*$.*

Proof. Denote the variance

$$\mathcal{F}(t) = \int_{\mathbb{R}} (q - \tilde{q}(t))^2 f(t,q)dq, \tag{3.2}$$

then

$$\begin{aligned}
\frac{d\mathcal{F}}{dt} &= \int_{\mathbb{R}} (q-\tilde{q})^2 f_t + 2(\tilde{q}-q)\tilde{q}_t f dq = \int_{\mathbb{R}} (q-\tilde{q})^2 f_t dq = \frac{1}{\epsilon}\int_{\mathbb{R}} (q-\tilde{q})^2 [(q-q^*)f]_q dq \\
&= -\frac{2}{\epsilon}\int_{\mathbb{R}} (q-q^*)(q-\tilde{q})f dq = -\frac{2}{\epsilon}\int_{\mathbb{R}} q(q-\tilde{q})f dq,
\end{aligned}$$

where the second and last equalities use the fact that $\int_{\mathbb{R}} qfdq = \tilde{q}$, and the forth one uses integration by parts. Notice that

$$\int_{\mathbb{R}} q^2 f dq - \int_{\mathbb{R}} q\tilde{q} f dq = \int_{\mathbb{R}} q^2 f dq \int_{\mathbb{R}} f dq - \left(\int_{\mathbb{R}} f q dq \right)^2 \geq 0$$

thanks to the Cauchy-Schwartz inequality, we have $\frac{d\mathcal{F}}{dt} \leq 0$. As a matter of fact, we have

$$\frac{d\mathcal{F}}{dt} = -\frac{2}{\epsilon} \int_{\mathbb{R}} q(q-\tilde{q}) f dq = -\frac{2}{\epsilon} \int_{\mathbb{R}} (q-\tilde{q})^2 f dq = -\frac{2}{\epsilon} \mathcal{F},$$

thus $\mathcal{F} \to 0$ as $t \to \infty$, and thus the equilibrium solution is $f = \delta(q - \tilde{q})$. Similarly, let $\mathcal{G}(t) = \int_{\mathbb{R}} (q-q^*)^2 f(t) dq$, then

$$\frac{d\mathcal{G}}{dt} = \int_{\mathbb{R}} (q-q^*)^2 f_t dq = \frac{1}{\epsilon} \int_{\mathbb{R}} (q-q^*)^2 \left[(q-q^*) f \right]_q dq = -\frac{2}{\epsilon} \int_{\mathbb{R}} (q-q^*)^2 f dq = -\frac{2}{\epsilon} \mathcal{G}.$$

Hence f converges to $\delta(q-q^*)$, and together with the above result leads to $\tilde{q}(t) \to q^*$. □

Now we return to the space inhomogeneous case

$$f_t + q f_x = \frac{1}{\epsilon} \left[(q-q^*) f \right]_q, \tag{3.3}$$

where similar arguments can apply to show

Proposition 2. *Let $f(t,x,q) > 0$ be the solution to the initial value problem of the space inhomogeneous equation (3.3). Assume $f(t,x,q)$ decays faster than $\frac{1}{|q|^2}$ as $|q| \to \infty$. Then as ϵ tends to 0, we formally have f converging to $\rho(t,x)\delta(q - q^*(t,x))$ and $\rho(t,x)\delta(q-\tilde{q}(t,x))$ with $\rho(t,x)$ and $\tilde{q}(t,x)$ defined in (1.3) and $q^*(t,x)$ defined in (2.9).*

Proof. The proof is similar to that in Proposition 1. Again denote

$$\mathcal{F}(t,x) = \int_{\mathbb{R}} (q - \tilde{q}(t,x))^2 f(t,x,q) dq, \tag{3.4}$$

then

$$\begin{aligned} \frac{d\mathcal{F}}{dt} &= -\frac{2}{\epsilon} \int (q-\tilde{q})(q-q^*) f dq - \int q f_x (q-\tilde{q})^2 dq \\ &= -\frac{2}{\epsilon} \int (q-\tilde{q})^2 f dq - \int q f_x (q-\tilde{q})^2 dq \\ &= -\frac{2}{\epsilon} \mathcal{F} - \int q f_x (q-\tilde{q})^2 dq. \end{aligned}$$

Thus in the limit $\epsilon \to 0$, we have $\mathcal{F} = 0$. Therefore, the dependence of f on q is a delta function $\delta(q - \tilde{q}(t,x))$. Then by conservation of mass, we have $f \to \rho(t,x)\delta(q-\tilde{q}(t,x))$. The convergence of f toward $\rho(t,x)\delta(q-q^*(t,x))$ similarly follows.

□

The above propositions provide insight on the situation wherein continuum system (2.9) is a good approximation to the kinetic model (2.5), that is, when γ is large enough. This is consistent with Theorem 4 in [2]. Moreover, since $\tilde{q}$ approaches q^* at the same time when f converges to the

mono-kinetic distribution, it suggests a mechanism to label the solutions in different regimes. That is, one can check

$$|\tilde{q}(t,x) - q^*(t,x)| > \epsilon_0 \tag{3.5}$$

for every x. If it holds, then this point falls into the kinetic regime, otherwise it is labeled as a continuum point. A reasonable choice of ϵ_0 is

$$\epsilon_0 = \max_x |q^*(0,x) - \tilde{q}(0,x)|. \tag{3.6}$$

Notice however, when the continuum model is no longer valid and $\tilde{q}(x)$ is very different from $q^*(x)$, there could still be $\tilde{q}(x) = q^*(x)$ at some points (such as their intersection). Therefore, to avoid mislabeling such points as continuum regime, we propose another criteria to accompany (3.5) :

$$\rho(x) > \rho_{\max}. \tag{3.7}$$

This means that if the density is beyond a threshold, which in analogy with the agent based model means two particles are too close, we need to switch on the kinetic solver. Here the choice of $\rho_{\max}$ is problem dependent. The indicator (3.5) (3.7) will be used for both the transition from kinetic to continuum or continuum to kinetic regimes.

Remark 3. Since the mono-kinetic distribution $\rho(t,x)\delta(q-\tilde{q}(t,x))$ can be considered as a local equilibrium, a natural criteria from kinetic to continuum would be $\|f(t,x,q)-\rho(t,x)\delta(q-\tilde{q}(t,x))\|_q < \epsilon_1$ for some small constant ϵ_1. However, one can only approximate the $\delta-$function, which makes such a measure very sensitive to the way we do the approximation. So, we will not use this criteria but stick to (3.5) (3.7) for both transitions.

3.2 Space and velocity discretization

In this section, we summarize numerical discretization of both kinetic equation (2.5) and continuum system (2.9), and postpone the interface condition to the next section. In fact, the choice of discretization is not unique, and most shock capturing methods for hyperbolic systems will apply.

Divide the spatial and velocity domain into a number of cells $[x_{j-\frac{1}{2}}, x_{j+\frac{1}{2}}]$ and $[q_{k-\frac{1}{2}}, q_{k+\frac{1}{2}}]$, where $j,\ k \in \mathbb{Z}$. Each cell is centered at x_j or q_k with a uniform length Δx or Δq. Denote $f^n_{j,k} = f(t^n, x_j, q_k)$, then a first order upwind scheme of (2.5) reads

$$\partial_t f_{j,k} + \frac{\eta_{j+\frac{1}{2},k} - \eta_{j-\frac{1}{2},k}}{\Delta x} + \gamma \frac{\xi_{j,k+\frac{1}{2}} - \xi_{j,k-\frac{1}{2}}}{\Delta q} = 0, \tag{3.8}$$

where

$$\begin{aligned} \eta_{j+\frac{1}{2},k} &= \frac{|q_k| + q_k}{2} f_{j,k} + \frac{q_k - |q_k|}{2} f_{j+1,k} \\ &:= \eta^+_{j,k} + \eta^-_{j+1,k}, \end{aligned} \tag{3.9}$$

$$\begin{aligned} \xi_{j,k+\frac{1}{2}} &= \frac{\left|q^*_j - q_{k+\frac{1}{2}}\right| + \left(q^*_j - q_{k+\frac{1}{2}}\right)}{2} f_{j,k} + \frac{\left(q^*_j - q_{k+\frac{1}{2}}\right) - \left|q^*_j - q_{k+\frac{1}{2}}\right|}{2} f_{j,k+1} \\ &:= \xi^+_{j,k} + \xi^-_{j,k+1}. \end{aligned} \tag{3.10}$$

Here we have used edge-values for the velocity discretization [29] and $q_{k+\frac{1}{2}} = \frac{q_k + q_{k+1}}{2}$.

To be consistent with the kinetic equation, we use a kinetic vector splitting method [14, 35, 21] for the continuum system. That is, multiplying (3.8) by $(1,q)^T$ and integrate with respect to q, we have

$$\partial_t U_j + \frac{F_{j+\frac{1}{2}} - F_{j-\frac{1}{2}}}{\Delta x} = S_j, \tag{3.11}$$

where

$$\begin{aligned}
U_j &= (\ \rho_j, \rho_j \tilde{q}_j\ )^T, && (3.12)\\
F_{j+\frac{1}{2}} &= \int (1,q)^T \frac{q+|q|}{2}\rho_j \delta(q-\tilde{q}_j)dq + \int (1,q)^T \frac{q-|q|}{2}\rho_{j+1}\delta(q-\tilde{q}_{j+1})dq \\
&= \left(\frac{\tilde{q}_j+|\tilde{q}_j|}{2}\rho_j + \frac{\tilde{q}_{j+1}-|\tilde{q}_{j+1}|}{2}\rho_{j+1},\ \tilde{q}_j\frac{\tilde{q}_j+|\tilde{q}_j|}{2}\rho_j + \tilde{q}_{j+1}\frac{\tilde{q}_{j+1}-|\tilde{q}|_{j+1}}{2}\rho_{j+1}\right)^T \\
&:= F_j^+ + F_{j+1}^-, && (3.13)\\
S_j &= (\ 0, \gamma\rho_j(q_j^* - \tilde{q}_j)\ )^T. && (3.14)
\end{aligned}$$

The extension to high resolution in space is straightforward using a slope limiter. More precisely, denote

$$\eta_{j+\frac{1}{2},k} = \eta^+_{j+\frac{1}{2},k} + \eta^-_{j+\frac{1}{2},k}, \tag{3.15}$$

then

$$\eta^+_{j+\frac{1}{2},k} = \eta^+_{j,k} + \frac{\Delta x}{2}\sigma^+_{j,k}, \qquad \sigma^+_{j,k} = \frac{\eta^+_{j+1,k}-\eta^+_{j,k}}{\Delta x}\varphi\left(\frac{\eta^+_{j,k}-\eta^+_{j-1,k}}{\eta^+_{j+1,k}-\eta^+_{j,k}}\right), \tag{3.16}$$

$$\eta^-_{j+\frac{1}{2},k} = \eta^-_{j+1,k} - \frac{\Delta x}{2}\sigma^-_{j+1,k}, \qquad \sigma^-_{j,k} = \frac{\eta^-_{j,k}-\eta^-_{j-1,k}}{\Delta x}\varphi\left(\frac{\eta^-_{j+1,k}-\eta^-_{j,k}}{\eta^-_{j,k}-\eta^-_{j-1,k}}\right), \tag{3.17}$$

where φ is the slope limiter function such as the Van Leer function [29]

$$\varphi(\theta) = \frac{|\theta|+\theta}{1+|\theta|}. \tag{3.18}$$

Similarly for the continuum system (3.11), the flux is computed as $F_{j+\frac{1}{2}} = F^+_{j+\frac{1}{2}} + F^-_{j+\frac{1}{2}}$, where $F^\pm_{j+\frac{1}{2}}$ are defined in the same manner as that in (3.16) (3.17). That is,

$$F^+_{j+\frac{1}{2},k} = F^+_{j,k} + \frac{\Delta x}{2}\sigma^+_{j,k}, \qquad \sigma^+_{j,k} = \frac{F^+_{j+1,k}-F^+_{j,k}}{\Delta x}\varphi\left(\frac{F^+_{j,k}-F^+_{j-1,k}}{F^+_{j+1,k}-F^+_{j,k}}\right), \tag{3.19}$$

$$F^-_{j+\frac{1}{2},k} = F^-_{j+1,k} - \frac{\Delta x}{2}\sigma^-_{j+1,k}, \qquad \sigma^-_{j,k} = \frac{F^-_{j,k}-F^-_{j-1,k}}{\Delta x}\varphi\left(\frac{F^-_{j+1,k}-F^-_{j,k}}{F^-_{j,k}-F^-_{j-1,k}}\right). \tag{3.20}$$

For kinetic equation (3.8), to construct a second order scheme in velocity, we add a flux limiter [30]. Then (3.8) is modified as

$$f^{n+1}_{j,k} = f^n_{j,k} - \frac{\Delta t}{\Delta x}\left(\eta^n_{j+\frac{1}{2},k} - \eta^n_{j-\frac{1}{2},k}\right) - \gamma\frac{\Delta t}{\Delta q}\left(\xi^n_{j,k+\frac{1}{2}} - \xi^n_{j,k-\frac{1}{2}}\right) - \gamma\frac{\Delta t}{\Delta q}\left(C^n_{j,k+\frac{1}{2}} - C^n_{j,k-\frac{1}{2}}\right). \tag{3.21}$$

Here $C_{j,k+\frac{1}{2}}$ is the corrector defined as

$$C_{j,k+\frac{1}{2}} = \frac{1}{2}|s_{j,k+\frac{1}{2}}|\left(1 - \frac{\Delta t}{\Delta q}|s_{j,k+\frac{1}{2}}|\right)\tilde{W}_{j,k+\frac{1}{2}}, \tag{3.22}$$

where $s_{j,k-\frac{1}{2}} = q_j^* - q_{k-\frac{1}{2}}$, $W_{j,k-\frac{1}{2}} = f_{j,k} - f_{j,k-\frac{1}{2}}$, and $\tilde{W}_{j,k-\frac{1}{2}} = W_{j,k-\frac{1}{2}}\varphi\left(\frac{W_{j,\mathbf{k}-\frac{1}{2}}}{W_{j,k-\frac{1}{2}}}\right)$. The subscript $\mathbf{k}$ is $k-1$ if $s_{j,k-\frac{1}{2}} > 0$ and $k+1$ if $s_{j,k-\frac{1}{2}} < 0$. φ is again the VanLeer function (3.18).

3.3 Interface condition

This section is concerned with the connection between two cells of different type. Denote $j = J$ such that $j < J$ is in the kinetic regime and $j \geq J$ is in the continuum regime, then we propose the following interface condition.

- To compute f_{J-1} via (3.8), we need to prescribe f_J at the last time step. Since f_J falls into the continuum regime, this can be done simply by using the *local equilibrium*. Namely

$$f_J(q) = \rho_J \delta(q - \tilde{q}_J). \tag{3.23}$$

- To compute ρ_J and $\tilde{q}_J$ via (3.11), we need ρ_{J-1} and $\tilde{q}_{J-1}$ from the last step. This is done by taking the moments of f_{J-1} thanks to the relationship (1.3). More precisely, we have

$$\rho_{J-1} = \int f_{J-1}(q)dq, \qquad \rho_{J-1}\tilde{q}_{J-1} = \int q f_{J-1}(q)dq. \tag{3.24}$$

Remark 4. This simple choice of interface condition is inspired by the fact that density and macroscopic velocity should undergo a *continuous* transition. Similar conditions have been used in [18] for rarefied gas dynamics. However, if we want to deal with the cases when γ has a discontinuous or sharp transition in magnitude, different interface conditions may need to be used to take into account the possible interface layer, and this is beyond the scope of the current paper.

Now the final algorithm is in order. At time t^n, denote by C^n the collection of cells that are in the continuum regime, i.e., $[x_{j-\frac{1}{2}}, x_{j+\frac{1}{2}}]_{j\in C^n}$ is in continuum regime, and by K^n the collection of cells in the kinetic regime, where $C^n \cup K^n = X = \{1, 2, ...N_x\}$. We have $(\rho_j^n, \tilde{q}_j^n)$ for $j \in C^n$, and f_j^n for $j \in K^n$.

- Compute q_j^* for all j and $\tilde{q}_j$, ρ_j for $j \in K^n$ via a discrete version of (1.3).
- Find the set K^{n+1} of all j such that $|q_j^* - \tilde{q}_j| > \epsilon_0$ or $\rho_j > \rho_{\max}$, which is the new kinetic regimes. Then the new continuum regime is $C^{n+1} = X \backslash K^{n+1}$.
- For $j \in K^{n+1}\backslash K^n$, compute $f_j^n = \rho_j \delta(q - \tilde{q}_j^n)$, where δ is approximated using (5.1).
- Evolve $(\rho_j^{n+1}, \tilde{q}_j^{n+1})$ for $j \in C^n$ from (3.11) and use interface condition (3.24) when necessary.
- Evolve f_j^{n+1} for $j \in K^{n+1}$ from (3.8) and use interface condition (3.23) when necessary.

4 A level set method

As explored in [2], the solution to the nonlinear hyperbolic system (2.9) often develops shocks in finite time. Viscosity solutions selected by scheme (3.11)–(3.14) (or other shock capturing schemes) are not appropriate in treating this particular dynamic. Instead, multivalued solutions that are determined by the fear level and corresponding crossing waves are the physically relevant ones. In this section, we develop a level set method that is capable of capturing the multivalued solution for the continuum system.

Recall the continuum system

$$\rho_t + (\rho\tilde{q})_x = 0, \tag{4.1}$$

$$\tilde{q}_t + \tilde{q}\tilde{q}_x = \gamma(q^* - \tilde{q}), \qquad q^* = \frac{\int \kappa(|x-y|)\rho(y)\tilde{q}(y)dy}{\int \kappa(|x-y|)\rho(y)dy}. \tag{4.2}$$

First we form a level set function $\Phi(t, x, p)$ such that the multivalued $\tilde{q}(t, x)$ can be realized as its zero level set, i.e.,

$$\Phi(t, x, p) = 0 \text{ at } p = \tilde{q}(t, x) \qquad \text{or} \qquad \Phi(t, x, \tilde{q}(t, x)) \equiv 0. \tag{4.3}$$

The remaining derivation follows that in [9, 26, 24]. Taking the time derivative of (4.3), one has

$$\partial_t\Phi + \partial_p\Phi\partial_t\tilde{q} = 0,$$

which becomes $\partial_t\Phi + \partial_p\Phi\left(-\tilde{q}\tilde{q}_x + \gamma(q^* - \tilde{q})\right) = 0$ thanks to (4.2). Then the level set equation in the phase space follows

$$\partial_t\Phi + \partial_p\Phi\left(-pp_x + \gamma(p^* - p)\right) = 0. \tag{4.4}$$

Taking the spatial derivative of (4.3), one has $\partial_x\Phi + \partial_p\Phi\partial_x\tilde{q} = 0$, thus

$$\partial_x\tilde{q} = -\frac{\partial_x\Phi}{\partial_p\Phi}. \tag{4.5}$$

Plugging (4.5) into (4.4) leads to

$$\partial_t\Phi + p\partial_x\Phi + \gamma\partial_p\Phi(p^* - p) = 0, \tag{4.6}$$

where $p^*(t, x)$ depending on the density will be defined later (see (4.11)). For smooth initial data $\tilde{q}_0(x)$, the initial condition for Φ is

$$\Phi(0, x, p) = p - \tilde{q}_0(x); \tag{4.7}$$

while for discontinuous $\tilde{q}_0(x)$ such as Riemann initial data, $\Phi(0, x, p)$ should be chosen as the signed distance function to the interface $p = \tilde{q}_0(x)$ [26]. Now, we need to derive the evolution equation for density ρ. Since $\tilde{q}$ is multivalued, ρ can be multivalued too. Denote $\rho(t, x) \equiv \hat{\rho}(t, x, \tilde{q}(t, x))$, as $\rho(t, x)$ solves (4.1), $\hat{\rho}$ satisfies the following equation

$$\partial_t\hat{\rho} + \hat{\rho}\partial_x\tilde{q} + \tilde{q}\partial_x\hat{\rho} + \partial_p\hat{\rho}\left(\partial_t\tilde{q} + \tilde{q}\partial_x\tilde{q}\right) = 0.$$

Then plug (4.5) and (4.2) into the above equation, we have

$$\partial_t\hat{\rho} + p\partial_x\hat{\rho} + \gamma(p^* - p)\partial_p\hat{\rho} = \hat{\rho}\frac{\Phi_x}{\Phi_p}, \tag{4.8}$$

where we have again used $p = \tilde{q}$. Here the drawback of equation (4.8) is that Φ_p can be zero, which makes its right hand side singular. Notice, however, that the physically relevant density should not be multivalued, so, inspired by [24], we consider it to be the projection of its value in phase space onto the curve $\Phi = 0$, i.e.,

$$\bar{\rho}(t,x) = \int \hat{\rho}(t,x,p)\delta(\Phi(p))|\Phi_p|dp. \tag{4.9}$$

Similarly the total fear is defined as

$$\bar{Q}(t,x) = \int p\hat{\rho}(t,x,p)\delta(\Phi(p))|\Phi_p|dp, \tag{4.10}$$

and thus

$$p^*(t,x) = \frac{\int (\kappa * \hat{\rho})\, p\delta(\Phi(p))|\Phi_p|dp}{\int (\kappa * \hat{\rho})\, \delta(\Phi(p))|\Phi_p|dp}. \tag{4.11}$$

Now, we define a new quantity

$$g(t,x,p) = \hat{\rho}(t,x,p)|\Phi_p(t,x,p)|. \tag{4.12}$$

As always, we need to write down the evolution equation for g. To this end, taking the derivative of (4.6) with respect to p, we obtain the following equation for Φ_p:

$$\partial_t \Phi_p + p\partial_x \Phi_p + \gamma(p^* - p)\partial_p \Phi_p = -\Phi_x + \gamma\Phi_p. \tag{4.13}$$

Then g defined in (4.12) solves

$$\begin{aligned} & \partial_t g + p\partial_x g + \gamma(p^* - p)\partial_p g \\ = \;& |\Phi_p|\left(\partial_t\hat{\rho} + p\partial_x\hat{\rho} + \gamma(p^* - p)\partial_p\hat{\rho}\right) + \hat{\rho}\left(\partial_t|\Phi_p| + p\partial_x|\Phi_p| + \gamma(p^* - p)\partial_p|\Phi_p|\right) \\ = \;& \hat{\rho}\frac{\Phi_x}{\Phi_p}|\Phi_p| + \hat{\rho}\left(-\Phi_x + \gamma\Phi_p\right)\operatorname{sgn}(\Phi_p) \\ = \;& \gamma\hat{\rho}|\Phi_p| = \gamma g \end{aligned} \tag{4.14}$$

where the second equality uses (4.8) and (4.13). The initial condition for g reads as follows

$$g(0,x,p) = \rho_0(x)|\Phi_p(0,x,p)|, \tag{4.15}$$

and if $\Phi(0,x,p)$ takes the form (4.7), then $g(0,x,p) = \rho_0(x)$.

To summarize, one can solve (4.6) and (4.14) with initial conditions (4.7) and (4.15), respectively. Then $\tilde{q}$ takes the zero level set of $\Phi(t,x,p)$, and $\bar{\rho}(t,x)$ and $\bar{Q}(t,x)$ are computed via

$$\bar{\rho}(t,x) = \int g(t,x,p)\delta(\Phi(p))dp, \qquad \bar{Q}(t,x) = \int pg(t,x,p)\delta(\Phi(p))dp. \tag{4.16}$$

Remark 5. It is interesting to point out that g solves the same equation as the kinetic probability density f, which suggests some similarity between the kinetic formulation and level set formulation, as both of them lift the dimension of the problem by one and unfold the multiple values. In fact, this relation has been observed in the literature of computing multivalued physical observables for geometrical optics, such as [24, 17, 23]. The advantage of the level set approach is that the high dimensionality from the phase space can be compensated for by using the local level set method (consult e.g., [16]), which reduces the computational complexity to that comparable to a computation in the physical space. By contrast, the kinetic formulation is amenable to the hybrid construction in Section 3 thanks to its close relation with the macroscopic quantities.

5 Numerical examples

We present several examples to validate our hybrid scheme and level set scheme in this section. In what follows, we always take $q \in [L_{q1}, L_{q2}]$ with $L_{q1} = 0$, $L_{q2} = 3$ and $x \in [L_{x1}, L_{x2}]$ with $L_{x1} = -50$, $L_{x2} = 50$. Let N_q and N_x be the number of points in q and x directions, respectively. We assume Neumann boundary conditions in both q and x. The time step Δt is chosen to satisfy the CFL condition $\Delta t = \frac{1}{2}\min\{\frac{\Delta x}{\max(q)}, \frac{\Delta q}{\gamma \max|q-q^*|}\}$. The delta function in the kinetic and hybrid scheme is approximated by

$$\delta(q) \sim E(q) = \frac{1}{\sqrt{\pi}R_0} e^{-\frac{q^2}{R_0^2}}, \qquad R_0 = 0.04 \tag{5.1}$$

when necessary. The interaction kernel we choose here takes the form

$$\phi(x) = \frac{1}{x^2 + R^2}\frac{R}{\pi}. \tag{5.2}$$

For the level set method, equation (4.6) and (4.14) are discretized similarly to the kinetic equation, and the delta function in computing the moments (4.16) takes the following approximation [24]

$$\delta_\eta(\phi(t,x,p)) = \begin{cases} \frac{1}{2\eta}\left(1 + \cos\frac{|\pi\phi(t,x,p)|}{\eta}\right) & |\phi(t,x,p)| \le \eta(t,x) \\ 0 & |\phi(t,x,p)| > \eta(t,x), \end{cases} \tag{5.3}$$

where $\eta(t,x) = 2\max_p(|\phi_p(t,x,p)|, 1)\Delta p$. Here $p \in [L_{q1}, L_{q2}]$ with $L_{q1} = 0$, $L_{q2} = 3$.

5.1 Asymptotic property

We first check the asymptotic behavior of the solution in the spatially homogeneous case. Consider equation $f_t = \gamma\left[(q-q^*)f\right]_q$ with *non-equilibrium* initial data $f(0,q) = \frac{3}{4}E(q-0.6) + \frac{1}{4}E(q-1.2)$ and a fixed $q^* = 1$. The first three figures in Fig. 1 display the evolution of $f(t,q)$ towards a local equilibrium. We start with a non-equilibrium initial data and as times goes on f concentrates on q^*. Fig. 1 on the bottom right presents the distance $|\tilde{q}(t) - q^*|$ in time with $\gamma = 1$, 2, and 3 respectively, where we see that bigger γ gives faster convergence rate as implied in the proof of Proposition 1.

Next we consider the spatially inhomogeneous case $f_t + qf_q = \gamma((q-q^*)f)_q$ with $\gamma = 100$ and initial data

$$\begin{gathered} \rho_I(0,x) = \sin\left(\tfrac{\pi x}{10}\right) + 2, \quad q_I(0,x) = \tfrac{1}{2}\left(3 - \tanh x\right), \\ f_I(x,q) = \rho_I(x)\left(\tfrac{1}{4}E(q - q_I(x) - 0.5) + \tfrac{3}{4}E(q - q_I(x) + 0.3)\right). \end{gathered} \tag{5.4}$$

Fig. 2 shows the evolution of $f(t,x,q)$. Initially $f_I(x,q)$ has two bumps in q for every x, as displayed in the left plot of Fig. 2. As time evolves, $f(t,x,q)$ starts to concentrate on $\tilde{q}(t,x)$, as confirmed by the right plot of Fig. 2 where the projection of f onto the (x,q) plane matches well with $\tilde{q}(t,x)$.

5.2 Convergence test

In this section, we perform a convergence test to check that the interface condition proposed in Section 3.3 will not violate the accuracy of the scheme. Consider the spatially inhomogeneous case with smoothed Riemann initial data

$$\rho_I(x) \equiv 1, \qquad q_I(x) = \frac{1}{2}\left(3 - \tanh(0.25x)\right), \qquad f_I(x,q) = \rho_I(x)E(q - q_I(x)). \tag{5.5}$$

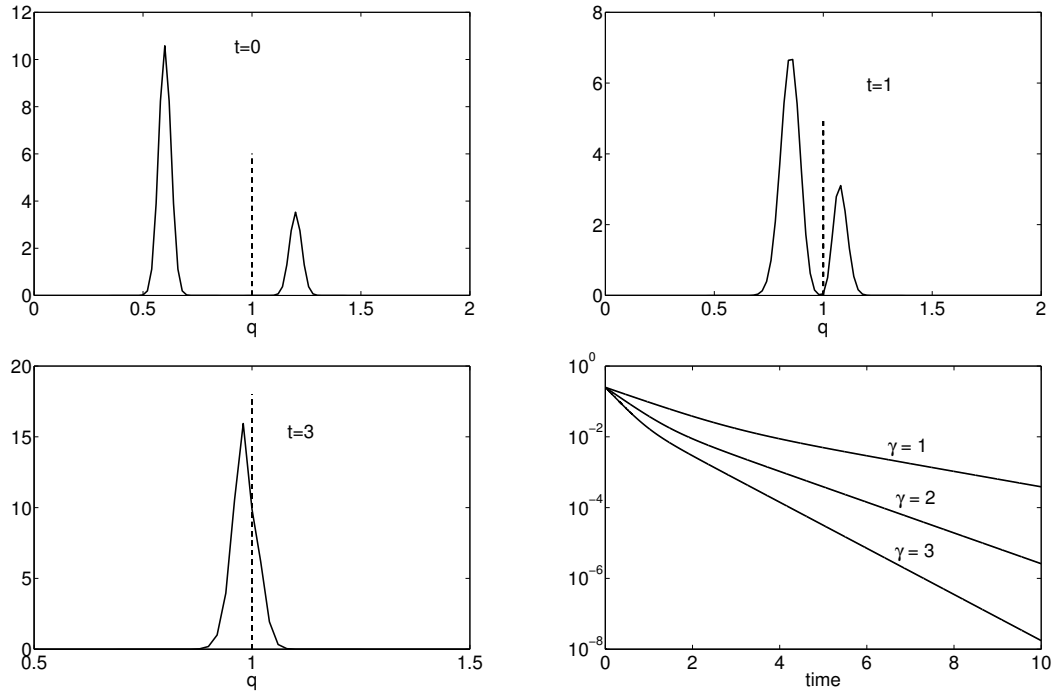

Figure 1: Solution to the spatially homogeneous equation (3.1) with non-equilibrium initial data (see the upper left figure). The next two figures display the solution with time $t = 1$ and 3, respectively. The dotted line in these three figures denotes q^*. The lower right plots the distance $|\tilde{q}(t) - q^*|$ versus time for $\gamma = 1$, 2 and 3.

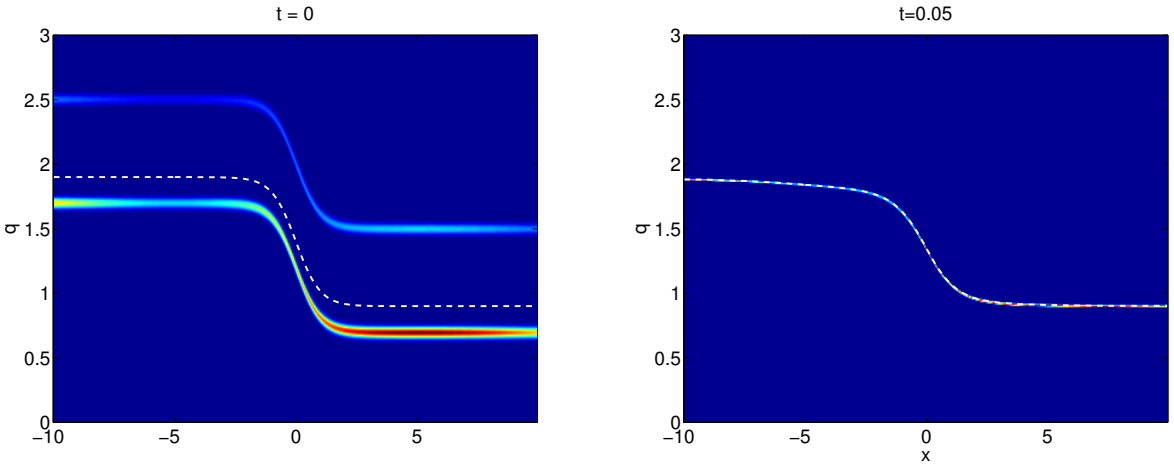

Figure 2: Plot of $f(t, x, q)$ to the space inhomogeneous equation with initial data (5.4). Left: initial configuration. Right: plot at time $t = 0.05$. Overlaid with the plot of macroscopic bulk fear $\tilde{q}(t, x)$ (dashed white line) at initial and final times.

We fix $\Delta q = 0.001$, and take the space mesh size $\Delta x = \frac{1}{10}, \frac{1}{20}, \frac{1}{40}, \frac{1}{80}, \frac{1}{160}$, respectively. In each case, we choose the time step $\Delta t = \frac{1}{2}\min\{\frac{\Delta x}{q_{max}}, \frac{\Delta q}{2q_{max}\gamma}\}$ to satisfy the CFL condition; here

$q_{max} = \max\{q\}$. The output time is $t_{max} = 0.1$, and we check the error in l^1 norm at $t = t_{\max}$,

$$error_{\Delta x} = \| \xi_{\Delta x}(t) - \xi_{2\Delta x}(t) \|_{l^1}, \tag{5.6}$$

where ξ can be f, ρ and Q. The results are collected in Fig. 3.

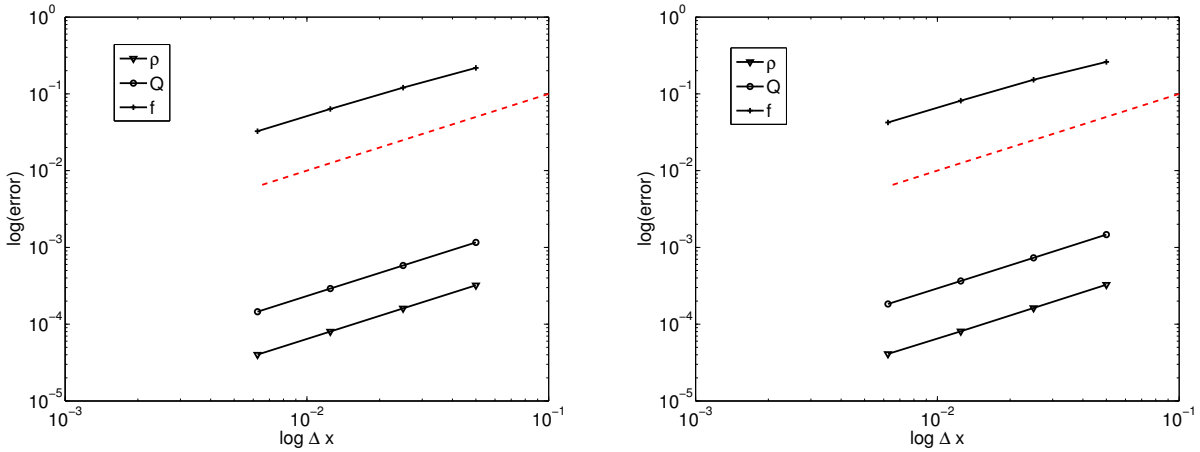

Figure 3: Plot of relative error (5.6) versus mesh size Δx. Here $x \in [-50, 50]$, $q \in [0, 3]$. Left: kinetic equation. Right: hybrid scheme with $\rho_{\max} = 1.01$, $\epsilon_0 = \max_x |q(0, x) - q^*(0, x)|$.

5.3 Riemann problem

In this section, we compare our hybrid scheme and level set method with the solutions to the kinetic and continuum systems for relatively long times after the crossing of characteristics. Here the initial density takes the form

$$\rho_I(x) = \frac{\rho_L}{2}\left(1 - \tanh(20x)\right) + \frac{\rho_R}{2}\left(1 + \tanh(20x)\right), \tag{5.7}$$

with $\rho_L = 2$ and $\rho_R = 1$, and initial fear is chosen as

$$q_I(x) = \frac{1}{2}\left(3 - \tanh(x)\right). \tag{5.8}$$

Our meshes are $\Delta x = 0.05$, $\Delta q = \Delta p = 0.01$. We use a moving frame with velocity $s = \frac{\sqrt{\rho_L} q_L + \sqrt{\rho_R} q_R}{\sqrt{\rho_L} + \sqrt{\rho_R}} = 1.5858$ (the formula for the shock speed obtained in [2]). The results are gathered in Fig. 4, where we compare the density $\rho(t, x)$, multivalued velocity $\tilde{q}(t, x)$, and averaged velocity $\frac{Q(t,x)}{\rho(t,x)}$. For the continuum system, it immediately gives $\tilde{q}\rho = Q$, while for the kinetic equation and level set formulation, the density $\rho(t, x)$ and total fear $Q(t, x)$ are calculated via (1.3) and (4.16), respectively. Here, a good agreement is observed among the kinetic system, hybrid scheme, and level set method, while the continuum system fails to capture the correct dynamics in the vicinity of the shock.

To better confirm that our hybrid scheme is able to detect different regimes automatically, we consider the following initial condition

$$\rho_I(x) = \frac{\rho_L}{2}\left(1 - \tanh(20(x - 30))\right) + \frac{\rho_R}{2}\left(1 + \tanh(20(x - 30))\right), \tag{5.9}$$

$$q_I(x) = \frac{1}{2}\left(2.6 - 0.8\tanh(x + 25) - 0.6\tanh(x - 30)\right) \tag{5.10}$$

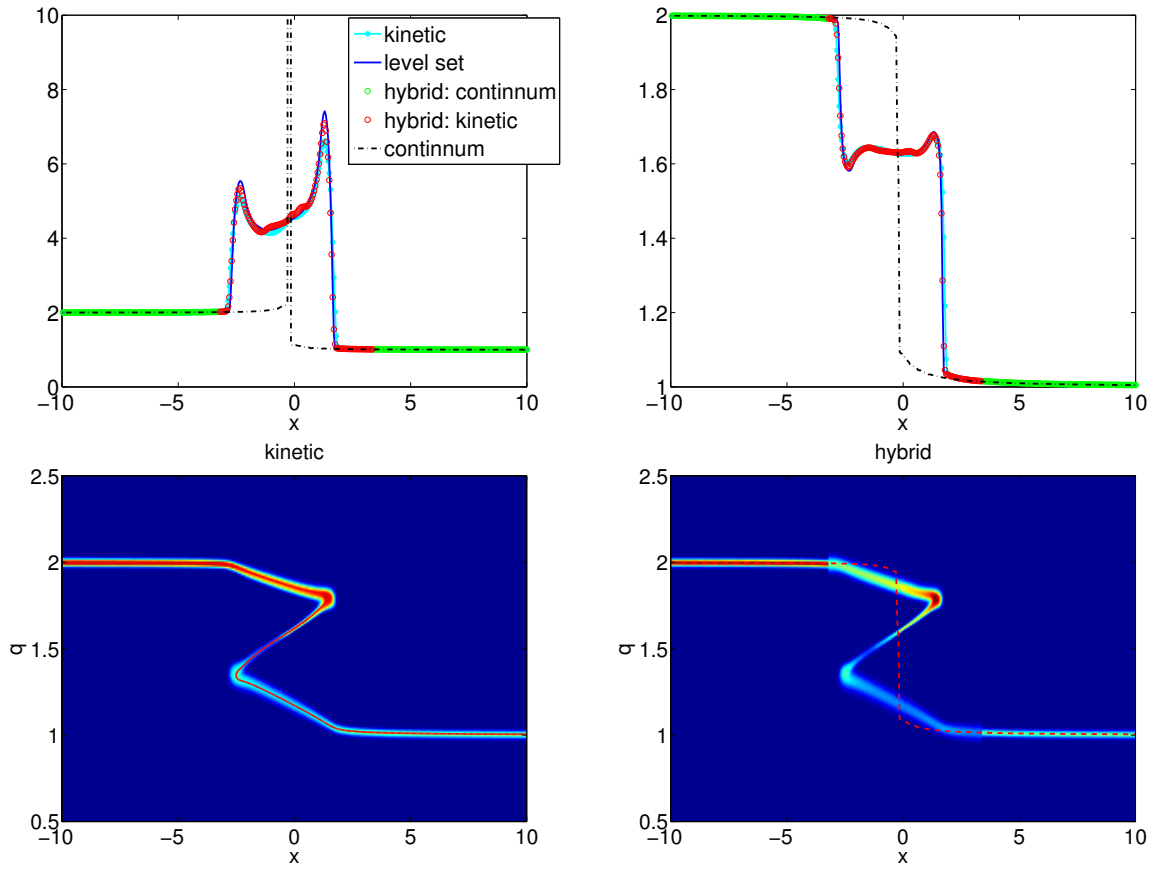

Figure 4: Solution to the Riemann initial data (5.5) (5.7) using the kinetic model, continuum model, and hybrid scheme. Upper left: plot of macroscopic density $\rho(t,x)$. Upper right: plot of macroscopic fear $\tilde{q}(t,x)$. Lower left: plot of the solution $f(t,x,q)$ to the kinetic equation, overlaid with the contour plot of the zero level set of $\Phi(t,x)$. Lower right: plot of $f(t,x,q)$ using the hybrid scheme, and the red dashed curve is $\tilde{q}(x)$ in the continuum model. Here $\gamma = 0.1$, $R = 0.1$, and final time is $t = 10$. For the hybrid scheme, we choose $\rho_{\max} = 2.1$ and $\epsilon_0 = 0.0489$ from (3.6).

with $\rho_L = 2$ and $\rho_R = 1$, which will produce a two shock solution. Again the parameters are as follows: $\gamma = 0.1$, $R = 0.1$, final time $t = 10$, and for the hybrid scheme, $\rho_{\max} = 2.1$ and $\epsilon_0 = 0.0299$ from (3.6). Here we use a moving mesh with speed $s = 1.6$, which is the speed for the left shock. With exactly the same grid, one sees in Fig. 5 that the solution from the continuum model is inferior to the hybrid scheme or level set method, both of which are in good match with the solution to the kinetic equation.

	Kinetic	Hybrid	Level set	Macroscopic
Example1	1458.7	504.7	1163.7	223.7
Example2	1509.9	525.5	1163.6	219.6

Table 1: Comparison of computational times (in seconds) for the above two examples. Example1 considers initial data (5.7) (5.8), and Example2 uses (5.9) (5.10); in all cases, $\Delta x = 0.05$, $\Delta q = \Delta p = 0.01$, $t = 10$.

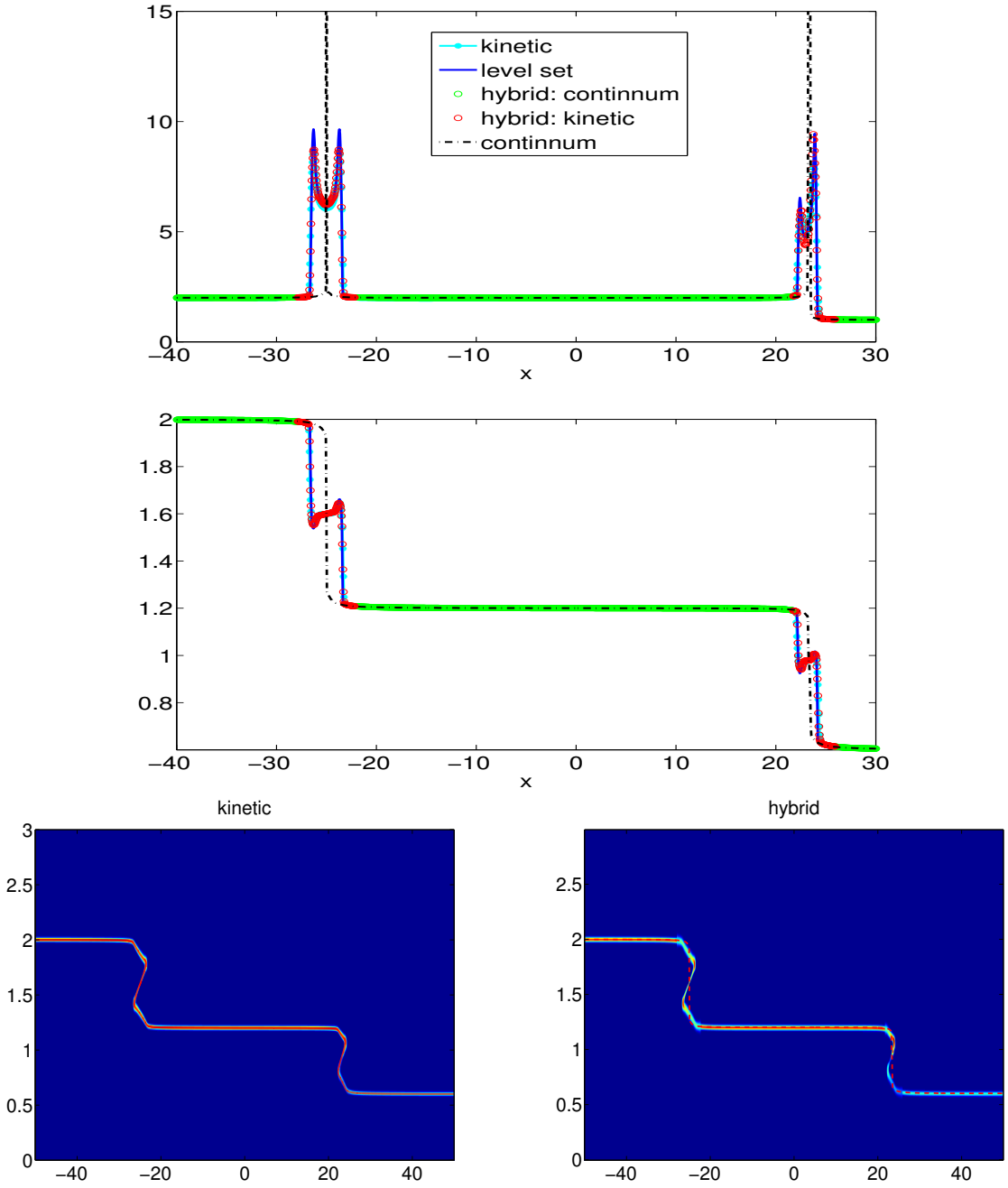

Figure 5: Solution to the Riemann initial data (5.9) (5.10) using the kinetic model, continuum model, hybrid scheme, and level set method. Top: plot of macroscopic density $\rho(t,x)$. Middle: plot of macroscopic fear $\tilde{q}(t,x) = \frac{Q(t,x)}{\rho(t,x)}$. Lower left: the solution $f(t,x,q)$ to the kinetic equation, overlaid with the contour zero of the level set method. Lower right: plot of $f(t,x,q)$ using the hybrid scheme, with the red dashed curve being $\tilde{q}(x)$ in the continuum model.

Concerning the computational time for different schemes with the same meshes ($\Delta x = 0.05$, $\Delta q = \Delta p = 0.01$), the cost for the hybrid scheme is comparable to the macroscopic solver and

almost 3 times faster than the full kinetic scheme. The level set method takes a longer time, but it can easily be accelerated using a local level set method. Model details are presented in Table 5.3. Here the implementation is in MATLAB and all the numerical results are obtained on a desktop computer with 12 cores and 2.67GHz CPU.

6 Conclusion

We constructed two numerical schemes for crowd dynamics with emotional contagion. Here the kinetic description provides better resolution than the macroscopic model whose viscosity solution becomes incorrect when the characteristics at the particle level cross. However, because of the high dimensionality, solving the kinetic equation is often expensive and sometimes unnecessary. Our first approach is a hybrid method that connects a continuum solver with a kinetic solver. The criteria that distinguishes two regimes is based on the macroscopic density and average fear level. The interface condition is proposed according to the continuity of the macroscopic quantities. Unlike previous research on hybrid schemes for kinetic and related problems, which focus on the Boltzmann type equation with a regular distribution (Maxwellian) as an equilibrium, our method here provides a new way to treat the singular (delta-like) equilibrium. As such types of equilibrium emerge in many other contexts such as biological swarming and opinion dynamics, it is desirable to apply our method to a broader scope. Our second approach is in the level set framework, which is inspired by the observation that the crossing of characteristics for particles results in a multi-valued solution in the fear for the continuum system. Although the so-derived level set equations live in a higher dimension than the macroscopic system, they can be solved just around the zero level set, which reduces the computational cost to that comparable to the macroscopic solver. Future research would be on deriving a more systematic expansion of the solution so that we can perform high order coupling. Rigorous convergence towards the monokinetic distribution as well as the convergence rate is still lacking and would be an interesting project.

Acknowledgements: This work is funded by ARO MURI grant W911NF-11-1-0332 and NSF grant CMMI-1435709.

References

[1] G. Bal and Y. Maday, *Coupling of transport and diffusion models in linear transport theory*, M2AN Math. Model. Numer. Anal., 36 (2002), pp. 69–86.

[2] A. Bertozzi, J. Rosado, M. Short, and L. Wang, *Contagion shock in one dimension*, J. Stat. Phys., 158 (2014), pp. 647–664.

[3] F. Bouchut, *On zero pressure gas dynamics*, in Advances in kinetic theory and computing, vol. 22 of Ser. Adv. Math. Appl. Sci., World Sci. Publ., River Edge, NJ, 1994, pp. 171–190.

[4] F. Bouchut, S. Jin, and X. Li, *Numerical approximations of pressureless and isothermal gas dynamics*, SIAM Journal on Numerical Analysis, 41, pp. pp. 135–158.

[5] J.-F. Bourgat, P. L. Tallec, B. Perthame, and Y. Qiu, *Coupling Boltzmann and Euler equations without overlapping*, In Domain Decomposition Methods in Science and Engineering, Contemp. Math., 157 (1994), pp. 377–398.

[6] Y. Brenier and E. Grenier, *Sticky particles and scalar conservation laws*, SIAM J. Numer. Anal., 35 (1998), pp. 2317–2328.

[7] J. A. Carrillo, M. Fornasier, G. Toscani, and F. Vecil, *Particle, kinetic, and hydrodynamic models of swarming*, Modeling and Simulation in Science, Engineering and Technology, (2010), pp. 297–336.

[8] G.-Q. Chen and H. Liu, *Formation of δ-shocks and vacuum states in the vanishing pressure limit of solutions to the Euler equations for isentropic fluids*, SIAM J. Math. Anal., 34 (2003), pp. 925–938.

[9] L. Cheng, H. Liu, and S. Osher, *Computational high frequency wave propagation using the level set method, with applications to the semi-classical limit of Shrodinger equations*, Comm. Math. Sci., 1 (2003), pp. 593–621.

[10] A. Chertock and A. Kurganov, *Computing multivalued solutions of pressureless gas dynamics by deterministic particle methods*, Commun. Comput. Phys., 5 (2009), pp. 565–581.

[11] F. Coquel, S. Jin, J. Liu, and L. Wang, *Well-posedness and singular limit of a semilinear hyperbolic relaxation system with a two-scale discontinuous relaxation rate*, Arch. Rat. Mech. Anal., 214 (2014), pp. 1051–1084.

[12] N. Crouseilles, P. Degond, and M. Lemou, *Hybrid kinetic/fluid models for non equilibrium systems*, C. R. Acad. Sci. Paris., 336 (2003), pp. 359–364.

[13] ——, *A hybrid kinetic-fluid model for solving the gas dynamics Boltzmann-BGK equation*, J. Comput. Phys., 199 (2004), pp. 776–808.

[14] S. M. Deshpande, *Kinetic theory based new upwind methods for inviscid compressible flows*, AIAA Paper, 86 (1986).

[15] G. Dimarco and L. Pareschi, *Hybrid multiscale methods ii. kinetic equations*, Multiscale Model. Simul., 6 (2008), p. 11691197.

[16] D.Peng, B. Merriman, S. Osher, H. Zhao, and M. Kang, *A PDE-based fast local level set method*, J. Comput. Phys., 155 (1999), pp. 410–438.

[17] B. Engquist and O. Runborg, *Multi-phase computations in geometrical optics*, J. Comput. Appl. Math., 74 (1996), pp. 175–192.

[18] F. Filbet and T. Rey, *A hierarchy of hybrid numerical methods for multiscale kinetic equations*, preprint.

[19] F. Golse, S. Jin, and C. Levermore, *The convergence of numerical transfer schemes in diffusive regimes i: The discrete-ordinate method*, SIAM J. Numer. Anal., 36 (1999), p. 13331369.

[20] ——, *A domain decomposition analysis for a two-scale linear transport problem*, Math. Model Num. Anal., 37 (2003), p. 869892.

[21] J. Hu and S. Jin, *On kinetic flux vector splitting schemes for quantum Euler equations*, Kinet. Relat. Models, 4 (2011), pp. 517–530.

[22] F. Huang and Z. Wang, *Well posedness for pressureless flow*, Comm. Math. Phys., 222 (2001), pp. 117–146.

[23] S. Jin and X. Li, *Multi-phase computations of the semiclassical limit of the schrodinger equation and related problems: Whit ham vs Wigner*, Physica D, 182 (2003), pp. 46–85.

[24] S. Jin, H. Liu, S. Osher, and R. Tsai, *Computing multivalued physical observables for the semiclassical limit of the Schrodinger equation*, J. Comput. Phys., 205 (2005), pp. 222–241.

[25] S. Jin, J. Liu, and L. Wang, *A domain decomposition method for semilinear hyperbolic systems with two-scale relaxations*, Math. Comp., 82 (2013), pp. 749–779.

[26] S. Jin and S. Osher, *A level set method for the computation of multivalued solutions to quasi-linear hyperbolic PDE's and Hamilton-Jacobi equations*, Comm. Math. Sci., 1 (2003), pp. 575–591.

[27] A. Klar, H. Neunzert, and J. Struckmeier, *Transition from kinetic theory to macroscopic fluid equations: A problem for domain decomposition and a source for new algorithm*, Transport Theory Statist. Phys., 29 (2000), pp. 93–106.

[28] P. LeTallec and F. Mallinger, *Coupling boltzmann and navier-stokes equations by half fluxes*, J. Comput. Phys., 136 (1997), pp. 51–67.

[29] R. J. LeVeque, *Numerical Methods for Conservation Laws. Birkhauser Verlag*, 1992.

[30] ——, *Finite Volume methods for hyperbolic problems. Cambridge University Press*, 2002.

[31] J. Li and H. Yang, *Delta-shocks as limits of vanishing viscosity for multidimensional zero-pressure gas dynamics*, Quart. Appl. Math., 59 (2001), pp. 315–342.

[32] J. Li and T. Zhang, *Generalized Rankine-Hugoniot relations of delta-shocks in solutions of transportation equations*, in Advances in nonlinear partial differential equations and related areas (Beijing, 1997), World Sci. Publ., River Edge, NJ, 1998, pp. 219–232.

[33] H. Liu and E. Tadmor, *Critical threshold in a convolution model for nonlinear conservation laws*, SIAM. J. Appl. Math., 33 (2001), pp. 930–945.

[34] S. Motsch and E. Tadmor, *A new model for self-organized dynamics and its flocking behavior*, Journal of Statistical Physics, Springer, 144 (2011), pp. 923–947.

[35] R. D. Reitz, *One-dimensional compressible gas dynamics calculations using the boltzmann equation*, J. Comput. Phys., 42 (1981), pp. 108–123.

[36] W. Sheng and T. Zhang, *The Riemann problem for the transportation equations in gas dynamics*, Mem. Amer. Math. Soc., 137 (1999), pp. viii+77.

[37] E. Tadmor and C. Tan, *Critical threshold in flocking hydrodynamics with nonlocal alignment*, Proceedings of the Royal Society, (2014).

[38] M. Tidriri, *New models for the solution of intermediate regimes in transport theory and radiative transfer: Eexistence theory, positivity, asymptotic analysis and applications*, J. Stat. Phys., 104 (2001), pp. 291–325.